

## Design, performance, and analysis of a measurement of optical properties of antarctic ice below 400 nm

---

### The IceCube Collaboration

(a complete list of authors can be found at the end of the proceedings)

*E-mail:* [jannes.brostean-kaiser@icecube.wisc.edu](mailto:jannes.brostean-kaiser@icecube.wisc.edu)

The IceCube Neutrino Observatory, located at the geographic South Pole, is the world's largest neutrino telescope, instrumenting 1 km<sup>3</sup> of Antarctic ice with 5160 photosensors to detect Cherenkov light. For the IceCube Upgrade, to be deployed during the 2022-23 polar field season, and the enlarged detector IceCube-Gen2 several new optical sensor designs are under development. One of these optical sensors, the Wavelength-shifting Optical Module (WOM), uses wavelength-shifting and light-guiding techniques to measure Cherenkov photons in the UV range from 250 nm to 380 nm. In order to understand the potential gains from this new technology, a measurement of the scattering and absorption lengths of UV light was performed in the SPICEcore borehole at the South Pole during the winter seasons of 2018/2019 and 2019/2020. For this purpose, a calibration device with a UV light source and a detector using the wavelength shifting technology was developed. We present the design of the developed calibration device, its performance during the measurement campaigns, and the comparison of data to a Monte Carlo simulation.

**Corresponding authors:** Jannes Brostean-Kaiser<sup>1</sup>\*

<sup>1</sup> *DESY Zeuthen, D-15738 Zeuthen*

\* Presenter

*37<sup>th</sup> International Cosmic Ray Conference (ICRC 2021)*

*July 12th – 23rd, 2021*

*Online – Berlin, Germany*

## 1. Introduction / Wavelength-shifting Optical Module

The IceCube Neutrino Observatory is a cubic-kilometer detector installed in the ice at the geographic South Pole at depths between 1,450 m and 2,450 m [1]. The detector was completed in 2010. To reconstruct direction, energy, and flavor of interacting neutrinos the Cherenkov radiation, emitted by charged secondary particles, is measured.

To improve the reconstruction of low energy neutrinos and the calibration of the instrumented ice, the IceCube Upgrade will be deployed in the austral summer 2022-2023. Seven additional strings will be deployed, including several types of novel optical modules.

Several of the new modules under development, are designed to measure Cherenkov radiation in the UV range. This improves the sensitivity of the modules since the number of emitted Cherenkov photons is proportional to one over the wavelength squared.

One of these UV-sensitive detectors is the Wavelength-shifting Optical Module (WOM)[2]. The WOM consists of a 76 cm long transparent (PMMA or quartz glass) tube with 10.6 cm diameter. The tube is coated with a wavelength-shifting paint [3] and connected to two photomultiplier tubes (PMTs), one on each side. The paint absorbs photons with a wavelength between 250 nm and 400 nm and reemits them at roughly 420 nm. The reemitted photons are guided via total internal reflection to one end of the tube and are detected by the PMTs.

## 2. Ice Properties

To understand the potential improvement of new optical modules, the surrounding material has to be calibrated in the sensitive range. The Antarctic ice originates in compacted snow turning to ice over long times. To measure scattering and absorption specifically, an in-situ measurement device, the UV calibration device (UV logger) has been built.

### 2.1 Absorption

In the visible spectrum down to 300 nm, the ice is mostly transparent, with absorption and scattering driven by impurities in the ice like dust, mineral, or soot [4]. In the very deep UV range a strong absorption occurs, the “Urbach tail” [5]. The exact cutoff wavelength is yet unknown but believed to be below 200 nm [6].

### 2.2 Scattering

Using the AMANDA detector the scattering and absorption coefficient could be calibrated down to 337 nm. Above 1300 m depth the scattering is dominated by small air bubbles converting to craigite in the IceCube depth range due to the ice pressure [7]. Below this so-called bubble-dominated region, the photons scatter on aforementioned impurities. The particles have varying radii between a few nanometers and several micrometer [4], which results in a mixture of Rayleigh and Mie-Scattering.

## 3. In-situ measurement in the SPICEcore hole

The in-situ measurements were done in the South Pole ice core hole (SPICEcore hole). It is an open borehole at about 1 km distance from the IceCube array with a depth of 1750 m [8] and 126

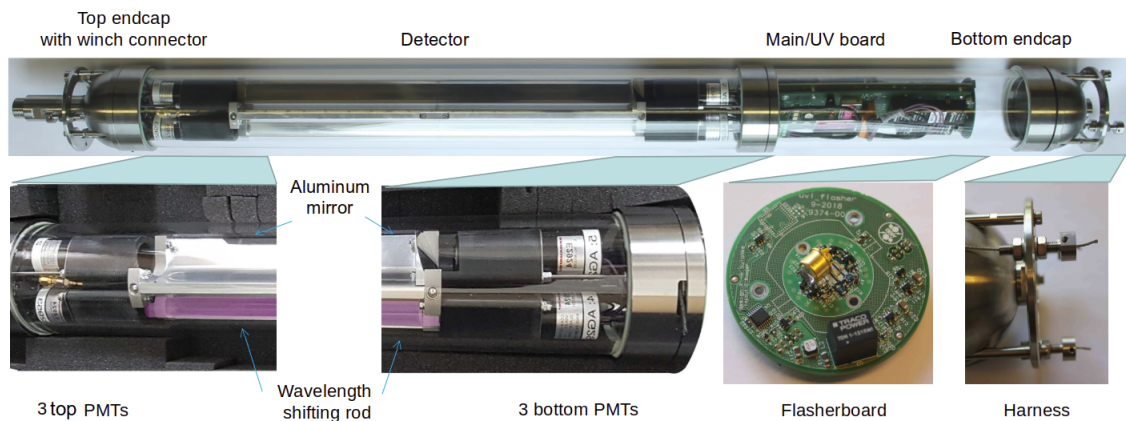


**Figure 1:** UV Calibration device with a detector, using PMTs, two open ones and four connected to wavelength shifting rods, a light source, capable of pulsing light with nanosecond pulse width and the read out electronic, stored in a quartz glass vessel with titanium endcaps and flanges .

38 mm diameter. During the drilling process, the hole was filled with Estisol 140, a synthetic ester fluid  
 39 that stays liquid in the South Pole environment. As its density is very similar to the surrounding  
 40 ice, it prevents the hole from collapsing and keeps the hole open for calibration measurements.

41 To measure in an open hole, the measurement device has to be the light emitter and detector  
 42 at the same time. The light is sent out into the ice in nanosecond short pulses. The detector  
 43 records the arrival time of the back-scattered photons. This time distribution can later be compared  
 44 to simulation to obtain the ice properties. Early simulations suggest that the rising edge of the  
 45 distribution is driven by the scattering coefficient, while the tail of the distribution is driven by the  
 46 absorption coefficient. These effects are visible in the Figures 5 a) and b).

47 Since a measurement with emitter and detector at the same place is more sensitive to backward  
 48 scattering than forward scattering, an additional future task will be the comparison between this  
 49 scattering measurement and former measurements with large detectors as IceCube or AMANDA.

50 In addition to the UV Calibration device several other in-situ measurements took place in the  
 51 two seasons as the Luminescence Logger [9], the Camera System [10] and the dust logger [11].

#### 52 4. Optimized UV calibration device

53 The device, designed for this measurement consists of a LED-based light source with different  
 54 wavelengths and a UV-sensitive detector. The detector is divided longitudinally into three segments  
 55 by aluminum mirrors. Two PMTs are placed in every segment (six in total), one near the light  
 56 source (bottom) and one on the top. In the two segments opposite of the LED, PMMA rods of  
 57 50 cm length and 2 cm diameter are connected to the PMTs. The rods are coated with a wavelength  
 58 shifting paint, developed for the WOM. In the segment facing the same direction as the LED the  
 59 PMTs are left open for direct photon detection. On the bottom PMT, an additional small mirror is  
 60 placed to increase the sensitivity of photons with only a few scattering processes. Figure 1 shows  
 61 the full logger with all components.

62 Most of the development and design have been  
 63 done prior to the first measurement season and  
 64 can be read up in previous works [12]. Only the  
 65 light source was altered between the two measure-  
 66 ment seasons. The light source is based on flasher  
 67 boards with one LED each. In the two measure-  
 68 ment seasons four flasher boards with wavelengths  
 69 of 245 nm, 278 nm, 310 nm and 370 nm were used.  
 70 The nanosecond light pulses are obtained using  
 71 a Kapustinsky Pulsar with adjustable light intensi-  
 72 ty. In the first measurement season an integrating  
 73 sphere [13] was used to create a well-defined emis-  
 74 sion profile. For the second measurement season  
 75 the integrating sphere was removed to increase the  
 76 number of emitted photons.

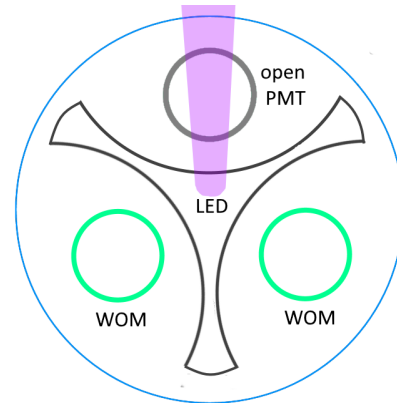
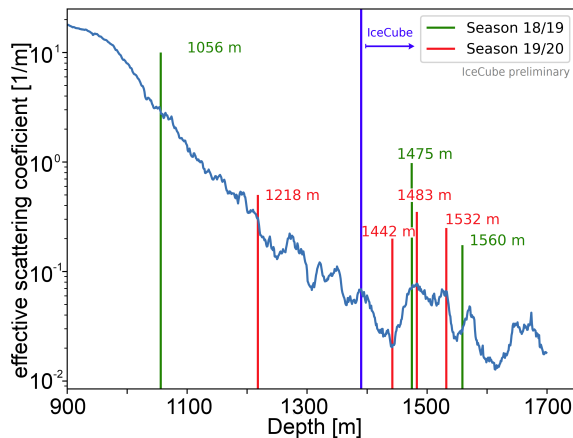


**Figure 2:** Cross section of the UV calibration device with the WOMs and open PMTs sketched according to the LED emission angle

## 77 5. Measurements



78  
 79  
 80  
 81  
 82  
 83  
 84  
 85  
 86  
 87  
 88  
**Figure 3:** All measurement depths of the two seasons,  
 89 together with the effective scattering coefficients[7],  
 90 shifted to compensate the ice tilt between IceCube and  
 91 SPICEcore. Depending on the depth the error of the ice  
 92 tilt can increase up to 30 m.

## 96 5.2 Second measurement season

97 The second measurement was performed in the austral summer 2019/2020. In total 4 mea-  
 98 surement days were taken with three different flasher boards, where the flasher board with 250 nm

The measurements were done in two seasons with a total of 4 wavelengths at 7 depths in the ice. Figure 3 shows the measurement depths together with the expected scattering coefficients.

### 5.1 First measurement season

In the austral summer 2018/2019 the first data set was collected on two days, at depths of 1056 m, 1475 m, and 1560 m, using both the 278 nm and 400 nm LED at each depth. Due to light intensity problems only the 278 nm LED provided useful data. During the whole measurement season one of the PMT channels, connected to a wavelength shifting rod did not record data. For some measurements the open PMTs picked up electric noise from the light source, but in every measurement at least 3 Channels recorded useful data.

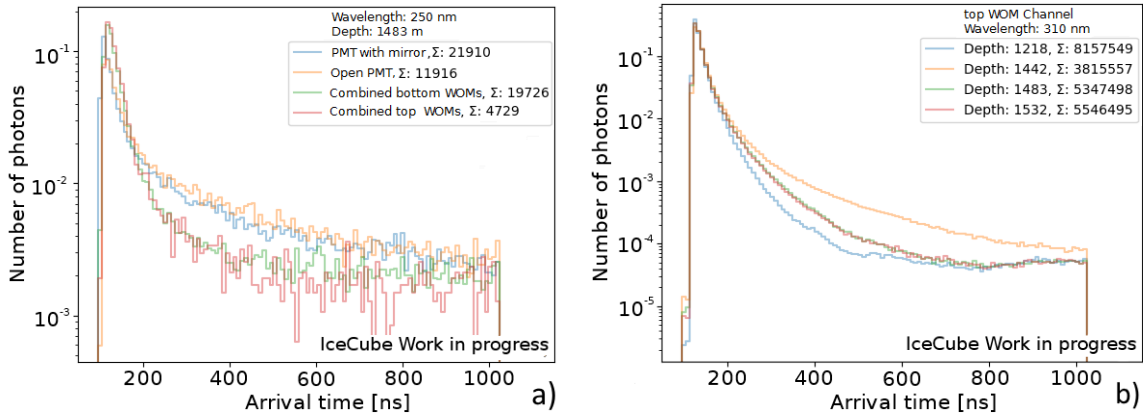


**Figure 4:** Prepared example data sets of the measurements a) with 250 nm at 1483 m depth for all channels and b) with 310 nm and the top WOM channel for all measured depths.

99 was used on two measurement days. The measurements were done at depths of 1218 m, 1442 m,  
100 1483 m and 1532 m.

101 The measurements with 250 nm, 310 nm and 370 nm all provided useful data. For the 250 nm  
102 measurement one channel connected to a wavelength shifting rod was not working.

### 103 5.3 Data preparation

104 To prepare the data for analysis it is represented in the form of histograms with 8 ns bins (limited  
105 by a firmware bug), and cut to a time window from 80 ns to 1050 ns. The PMTs connected to the  
106 wavelength shifting rods are summed for each side, to have only two WOM channels, one for the  
107 bottom PMTs (the side nearer to the light source) next to the PMT with the mirror and one for the  
108 top PMTs (further away from the light source).

109 Figure 4 shows two sorted and prepared example datasets. (a) displays all channels of one  
110 measurement with a wavelength of 245 nm at a depth of 1483 m, (b) displays the top WOM channel  
111 for all measured depths with 310 nm. From these examples, it is evident, that the WOM channels  
112 have a larger time spread due to the wavelength shifting. Also the different depths have visible  
113 differences in the histograms.

## 114 6. Data Analysis

115 The analysis is done by comparing the experimental data to Monte Carlo (MC) simulation with  
116 different absorption and scattering coefficients. The comparison to data is done using a binned  
117 maximum likelihood fit.

### 118 6.1 Simulation

119 The simulation models the experimental design in as much detail as possible. For the light  
120 emission, angular distribution, and wavelength spectrum of the LEDs datasheet values are interpo-  
121 lated.

122 The simulation follows the light path out of the calibration device through the quartz glass and  
123 Estisol into the ice using Fresnel equations. Every photon reaching the ice is assigned an absorption

124 and scattering length sampled from random exponential distributions with the absorption and scat-  
 125 tering coefficient as coefficients. After each scattering length, a scattering angle is sampled and the  
 126 photon receives a new direction and scattering length. After every scattering process, the traveled  
 127 path length is integrated and compared to the absorption length. After passing the assigned absorp-  
 128 tion length in the ice the photon is counted as absorbed in the ice. The scattering angle is highly  
 129 dependent on the scattering model. For the simulation, Mie-Scattering was tested, but found to be  
 130 impractical, since the experiment is mostly sensitive to backward scattering. Rayleigh scattering is  
 131 used instead. The angular distribution for Rayleigh scattering follows a  $(1 - \cos\vartheta)^2$ -distribution,  
 132 with  $\vartheta$  as the scattering angle.

133 Photons scattered back to the detector again pass through the Estisol and quartz glass into the  
 134 detector and are counted as detected when crossing a PMT or wavelength shifting rod. The transit  
 135 time spread of the different detection ways was measured in the laboratory and is dependent on the  
 136 position of the photon.

## 137 6.2 Maximum Likelihood fit

138 To analyze the measurements, the distribution of binned photon arrival times is compared to the  
 139 simulation. The comparison is done by calculating a test statistic  $TS$  for every simulation according  
 140 to the formula

$$TS = \sum_{i=1}^N \frac{(d_i - a_i \cdot N_d/N_a)^2}{d_i + a_i \cdot N_d^2/N_a^2} \quad (1)$$

141 where  $N$  is total number of bins in the measurement,  $d_i$  and  $a_i$  are the number of events in the bin  
 142  $i$  for the measurement  $d$  and the Monte-Carlo simulation  $a$  and  $N_d$  and  $N_a$  are the total number of  
 143 events in the measurement and Monte-Carlo simulation [14].

144 With this test statistic, a best fitting simulation with a given set of parameters can be found.  
 145 Figure 5 a) shows how the data of one depth, wavelength, and PMT-Channel connected to a WOM  
 146 and five simulations are matching up. Four simulations are done with a set of high or low scattering  
 147 and absorption parameters to show the boundaries of the chosen 2D scan. One simulation with a  
 148 set of medium coefficients is shown in red and gives the best fit with the smallest calculated  $TS$ .  
 149 Below the time distributions, the  $TS$  per bin is plotted, so to understand the influence of each part  
 150 of the distribution

151 To find a region of trustworthy minima the simulation with the lowest  $TS$  is re-simulated and  
 152 analysed 100 times to find a standard deviation  $\sigma$ . The true value for the parameters is supposed to  
 153 lie inside an area where the difference of the  $TS$  values to the minimum is smaller than  $\sigma$ , called  
 154 the  $1\sigma$  region. This method is used to compensate for the limited simulation time. Since the  
 155 number of simulated photons are smaller by a factor 10 to 100 it statistical error is mostly driven  
 156 by the simulation instead of the measurement. This represents only the statistical error and not the  
 157 systematic errors of the measurement.

## 158 6.3 Open issues

159 The analysis returns a well defined minimum for each channel of the measurement, but there  
 160 are still unsolved inconsistencies to be explained. Figure 6 a) and b) show two simplified simulation

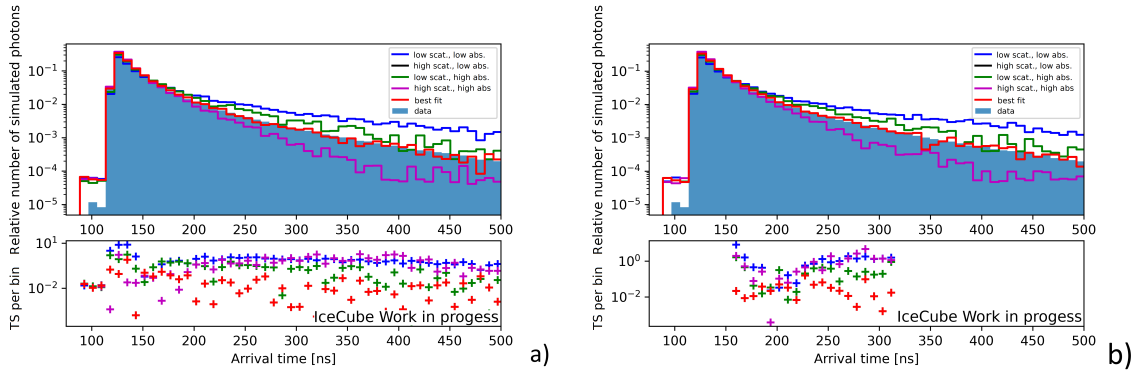


**Figure 5:** Dataset of a measurement with 5 simulations, 4 at the edges of the chosen parameter space and one best fit, a) for all bins with 10 or more entries, b) for a restricted time window of 150 ns - 300 ns.

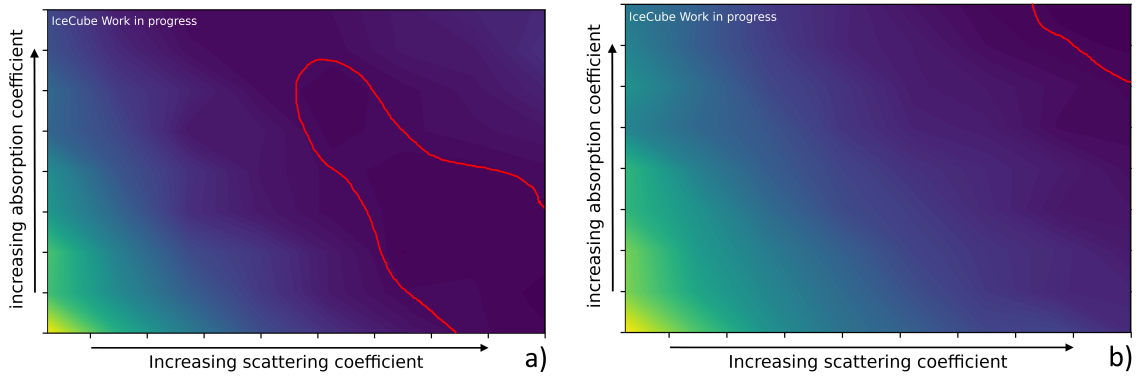


**Figure 6:** Simplified  $TS$  grid of several simulated sets of parameters compared to one data set for two PMT-channels of the same measurement.

161 grids of  $TS$  calculations as a function of absorption and scattering. Both axes depict about 1 order  
 162 of magnitude for each parameter. The red curve indicates the  $1\sigma$  region around the minimum.

163 The first unexplained observation is the differences between the PMT-channels. Comparing  
 164 the minima in Figure 6 a) and b) the  $\sigma$  regions are not overlapping. Therefore no definite minimum  
 165 connecting all channels of one measurement has yet been found. This questions the correctness of  
 166 the simulation and how well the experimental setup is understood.

167 Another concern is the size of the  $\sigma$  region. For some measurements as 6 a) it covers almost  
 168 the whole simulation grid. This and the form of the  $\sigma$  region indicate a strong correlation of the  
 169 two parameters. The choice of the scanned parameter space has to be therefore made very carefully  
 170 to not have a minimum on the borders of the scanned area.

171 To decouple the two parameters the histograms are restricted to a time window of 150 ns -  
 172 300 ns, where the distributions are believed to be mostly absorption driven. Figure 5 b) again  
 173 shows the best fit and several example simulations for this restricted time window. Figure 7 gives  
 174 again the simplified simulation grid with the  $\sigma$  region around the minimum, showing still the  
 175 same dependency of the two parameters. This leads to the conclusion that the two parameters  
 176 are not easily decoupled and the final results could be a combined extinction parameter instead of  
 177 independent absorption and scattering coefficients.

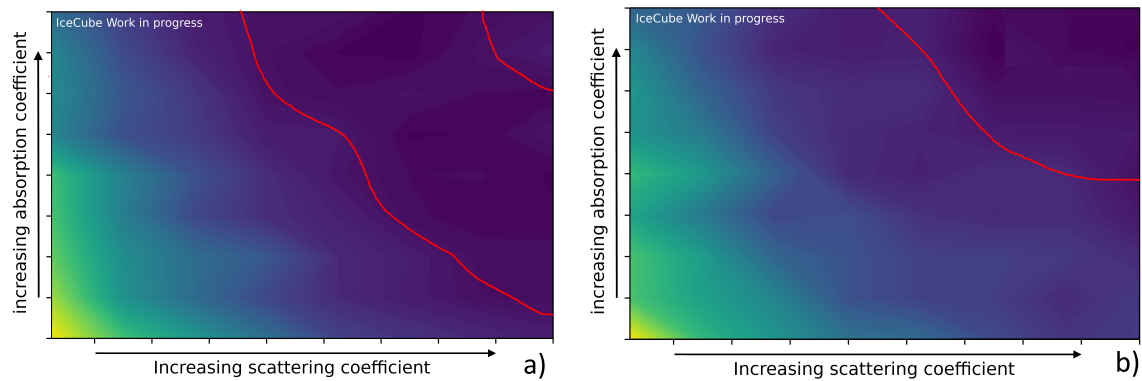


**Figure 7:** Simplified  $TS$  grid of several simulated sets of parameters compared to one data set for two PMT-channels of the same measurement with a restricted time window.

## 178 7. Outlook

179 In the future, the focus will be on increasing the understanding of the experimental setup to  
 180 understand and compensate for the differences in the measurement channels. This should lead to  
 181 a combined minimum for each data set on each measured wavelength and depth, which can be  
 182 compared to previous ice calibrations.

## 183 Acknowledgements

184 The author would like to thank the SPICEcore collaboration for providing the borehole, the US  
 185 Ice Drilling Program, the Antarctic Support Contractor and the NSF National Science Foundation  
 186 for providing the equipment to perform the measurement and for their support at South Pole.

## 187 References

- 188 [1] **IceCube** Collaboration, M. G. Aartsen *et al.* *JINST* **12** no. 03, (2017) P03012.  
 189 [2] **IceCube** Collaboration *PoS ICRC2017* (2017) 1052.  
 190 [3] **IceCube** Collaboration *PoS ICRC2021* (these proceedings) .  
 191 [4] Y. D. He and P. B. Price *J. Geophys. Res.: Atmos* **103** no. D14, (1998) 17041–17056.  
 192 [5] F. Urbach *Phys. Rev.* **92** no. 15, (1953) P01324.  
 193 [6] A. P. Minton *JPC* **75** (1971) 1162–1164.  
 194 [7] **IceCube** Collaboration, M. Ackermann *et al.* *JGR* **111** no. O3, (2006) .  
 195 [8] K. A. Casey *et al.* *Annals of Glaciology* **55** (1971) 137–146.  
 196 [9] **IceCube** Collaboration *PoS ICRC2019* (July 22, 2019) 983.  
 197 [10] **IceCube** Collaboration *PoS ICRC2021* (these proceedings) .  
 198 [11] M. Rongen, R. Bay, and S. Blot *The Cryosphere* **14** (08, 2020) 2537–2543.  
 199 [12] **IceCube** Collaboration *PoS ICRC2019* (2019) 847.  
 200 [13] **IceCube** Collaboration *PoS ICRC2021* (these proceedings) .  
 201 [14] B. Barlow *PCP* **77** no. 2, (1993) 219–228.

## 202 Full Author List: IceCube Collaboration

203 R. Abbasi<sup>17</sup>, M. Ackermann<sup>59</sup>, J. Adams<sup>18</sup>, J. A. Aguilar<sup>12</sup>, M. Ahlers<sup>22</sup>, M. Ahrens<sup>50</sup>, C. Alispach<sup>28</sup>, A. A. Alves Jr.<sup>31</sup>, N. M.  
 204 Amin<sup>42</sup>, R. An<sup>14</sup>, K. Andeen<sup>40</sup>, T. Anderson<sup>56</sup>, G. Anton<sup>26</sup>, C. Argüelles<sup>14</sup>, Y. Ashida<sup>38</sup>, S. Axani<sup>15</sup>, X. Bai<sup>46</sup>, A. Balagopal V.<sup>38</sup>,  
 205 A. Barbano<sup>28</sup>, S. W. Barwick<sup>30</sup>, B. Bastian<sup>59</sup>, V. Basu<sup>38</sup>, S. Baur<sup>12</sup>, R. Bay<sup>8</sup>, J. J. Beatty<sup>20,21</sup>, K.-H. Becker<sup>58</sup>, J. Becker Tjus<sup>11</sup>, C.  
 206 Bellenghi<sup>27</sup>, S. BenZvi<sup>48</sup>, D. Berley<sup>19</sup>, E. Bernardini<sup>59,60</sup>, D. Z. Besson<sup>34,61</sup>, G. Binder<sup>8,9</sup>, D. Bindig<sup>58</sup>, E. Blaufuss<sup>19</sup>, S. Blot<sup>59</sup>,  
 207 M. Boddenberg<sup>1</sup>, F. Bontempo<sup>31</sup>, J. Borowka<sup>1</sup>, S. Böser<sup>39</sup>, O. Botner<sup>57</sup>, J. Böttcher<sup>1</sup>, E. Bourbeau<sup>22</sup>, F. Bradascio<sup>59</sup>, J. Braun<sup>38</sup>, S.  
 208 Bron<sup>28</sup>, J. Brostean-Kaiser<sup>59</sup>, S. Browne<sup>32</sup>, A. Burgman<sup>57</sup>, R. T. Burley<sup>2</sup>, R. S. Busse<sup>41</sup>, M. A. Campana<sup>45</sup>, E. G. Carnie-Bronca<sup>2</sup>,  
 209 C. Chen<sup>6</sup>, D. Chirkin<sup>38</sup>, K. Choi<sup>52</sup>, B. A. Clark<sup>24</sup>, K. Clark<sup>33</sup>, L. Classen<sup>41</sup>, A. Coleman<sup>42</sup>, G. H. Collin<sup>15</sup>, J. M. Conrad<sup>15</sup>, P.  
 210 Coppin<sup>13</sup>, P. Correa<sup>13</sup>, D. F. Cowen<sup>55,56</sup>, R. Cross<sup>48</sup>, C. Dappen<sup>1</sup>, P. Dave<sup>6</sup>, C. De Clercq<sup>13</sup>, J. J. DeLaunay<sup>56</sup>, H. Dembinski<sup>42</sup>, K.  
 211 Deoskar<sup>50</sup>, S. De Ridder<sup>29</sup>, A. Desai<sup>38</sup>, P. Desati<sup>38</sup>, K. D. de Vries<sup>13</sup>, G. de Wasseige<sup>13</sup>, M. de With<sup>10</sup>, T. DeYoung<sup>24</sup>, S. Dharani<sup>1</sup>,  
 212 A. Diaz<sup>15</sup>, J. C. Díaz-Vélez<sup>38</sup>, M. Dittmer<sup>41</sup>, H. Dujmovic<sup>31</sup>, M. Dunkman<sup>56</sup>, M. A. DuVernois<sup>38</sup>, E. Dvorak<sup>46</sup>, T. Ehrhardt<sup>39</sup>, P.  
 213 Eller<sup>27</sup>, R. Engel<sup>31,32</sup>, H. Erpenbeck<sup>1</sup>, J. Evans<sup>19</sup>, P. A. Evenson<sup>42</sup>, K. L. Fan<sup>19</sup>, A. R. Fazely<sup>7</sup>, S. Fiedlschuster<sup>26</sup>, A. T. Fienberg<sup>56</sup>,  
 214 K. Filimonov<sup>8</sup>, C. Finley<sup>50</sup>, L. Fischer<sup>59</sup>, D. Fox<sup>55</sup>, A. Frankowski<sup>11,59</sup>, E. Friedman<sup>19</sup>, A. Fritz<sup>39</sup>, P. Fürst<sup>1</sup>, T. K. Gaisser<sup>42</sup>, J.  
 215 Gallagher<sup>37</sup>, E. Ganster<sup>1</sup>, A. Garcia<sup>14</sup>, S. Garrappa<sup>59</sup>, L. Gerhardt<sup>9</sup>, A. Ghadimi<sup>54</sup>, C. Glaser<sup>57</sup>, T. Glauch<sup>27</sup>, T. Glüsenskamp<sup>26</sup>, A.  
 216 Goldschmidt<sup>9</sup>, J. G. Gonzalez<sup>42</sup>, S. Goswami<sup>54</sup>, D. Grant<sup>24</sup>, T. Grégoire<sup>56</sup>, S. Griswold<sup>48</sup>, M. Gündüz<sup>11</sup>, C. Günther<sup>1</sup>, C. Haack<sup>27</sup>,  
 217 A. Hallgren<sup>57</sup>, R. Halliday<sup>24</sup>, L. Halve<sup>1</sup>, F. Halzen<sup>38</sup>, M. Ha Minh<sup>27</sup>, K. Hanson<sup>38</sup>, J. Hardin<sup>38</sup>, A. A. Harnisch<sup>24</sup>, A. Haungs<sup>31</sup>, S.  
 218 Hauser<sup>1</sup>, D. Hebecker<sup>10</sup>, K. Helbing<sup>58</sup>, F. Henningsen<sup>27</sup>, E. C. Hettinger<sup>24</sup>, S. Hickford<sup>58</sup>, J. Hignight<sup>25</sup>, C. Hill<sup>16</sup>, G. C. Hill<sup>2</sup>, K. D.  
 219 Hoffman<sup>19</sup>, R. Hoffmann<sup>58</sup>, T. Hoinka<sup>23</sup>, B. Hokanson-Fasig<sup>38</sup>, K. Hoshina<sup>38,62</sup>, F. Huang<sup>56</sup>, M. Huber<sup>27</sup>, T. Huber<sup>31</sup>, K. Hultqvist<sup>50</sup>,  
 220 M. Hünnefeld<sup>23</sup>, R. Hussain<sup>38</sup>, S. In<sup>52</sup>, N. Iovine<sup>12</sup>, A. Ishihara<sup>16</sup>, M. Jansson<sup>50</sup>, G. S. Japaridze<sup>5</sup>, M. Jeong<sup>52</sup>, B. J. P. Jones<sup>4</sup>, D. Kang<sup>31</sup>,  
 221 W. Kang<sup>52</sup>, X. Kang<sup>45</sup>, A. Kappes<sup>41</sup>, D. Kappesser<sup>39</sup>, T. Karg<sup>59</sup>, M. Kar<sup>27</sup>, A. Karle<sup>38</sup>, U. Katz<sup>26</sup>, M. Kauze<sup>38</sup>, M. Kellermann<sup>1</sup>, J. L.  
 222 Kelley<sup>38</sup>, A. Kheirandish<sup>56</sup>, K. Kin<sup>16</sup>, T. Kintscher<sup>59</sup>, J. Kiryluk<sup>51</sup>, S. R. Klein<sup>8,9</sup>, R. Koirala<sup>42</sup>, H. Kolanoski<sup>10</sup>, T. Kontrimas<sup>27</sup>, L.  
 223 Köpke<sup>39</sup>, C. Kopper<sup>24</sup>, S. Kopper<sup>54</sup>, D. J. Koskinen<sup>22</sup>, P. Koundal<sup>31</sup>, M. Kovacevich<sup>45</sup>, M. Kowalski<sup>10,59</sup>, T. Kozynets<sup>22</sup>, E. Kun<sup>11</sup>,  
 224 N. Kurahashi<sup>45</sup>, N. Lad<sup>59</sup>, C. Lagunas Gualda<sup>59</sup>, J. L. Lanfranchi<sup>56</sup>, M. J. Larson<sup>19</sup>, F. Lauber<sup>58</sup>, J. P. Lazar<sup>14,38</sup>, J. W. Lee<sup>52</sup>, K.  
 225 Leonard<sup>38</sup>, A. Leszczyńska<sup>32</sup>, Y. Li<sup>56</sup>, M. Lincetto<sup>11</sup>, Q. R. Liu<sup>38</sup>, M. Liubarska<sup>25</sup>, E. Lohfink<sup>39</sup>, C. J. Lozano Mariscal<sup>41</sup>, L. Lu<sup>38</sup>,  
 226 F. Lucarelli<sup>28</sup>, A. Ludwig<sup>24,35</sup>, W. Luszczak<sup>38</sup>, Y. Lyu<sup>8,9</sup>, W. Y. Ma<sup>59</sup>, J. Madsen<sup>38</sup>, K. B. M. Mahn<sup>24</sup>, Y. Makino<sup>38</sup>, S. Mancina<sup>38</sup>,  
 227 I. C. Mariš<sup>12</sup>, R. Maruyama<sup>43</sup>, K. Mase<sup>16</sup>, T. McElroy<sup>25</sup>, F. McNally<sup>36</sup>, J. V. Mead<sup>22</sup>, K. Meagher<sup>38</sup>, A. Medina<sup>21</sup>, M. Meier<sup>16</sup>, S.  
 228 Meighen-Berger<sup>27</sup>, J. Micaller<sup>24</sup>, D. Mockler<sup>12</sup>, T. Montaruli<sup>28</sup>, R. W. Moore<sup>25</sup>, R. Morse<sup>38</sup>, M. Moulai<sup>15</sup>, R. Naab<sup>59</sup>, R. Nagai<sup>16</sup>, U.  
 229 Naumann<sup>58</sup>, J. Necker<sup>59</sup>, L. V. Nguyen<sup>24</sup>, H. Niederhausen<sup>27</sup>, M. U. Nisa<sup>24</sup>, S. C. Nowicki<sup>24</sup>, D. R. Nygren<sup>9</sup>, A. Obertacke Pollmann<sup>58</sup>,  
 230 M. Oehler<sup>31</sup>, A. Olivas<sup>19</sup>, E. O'Sullivan<sup>57</sup>, H. Pandya<sup>42</sup>, D. V. Pankova<sup>56</sup>, N. Park<sup>33</sup>, G. K. Parker<sup>4</sup>, E. N. Paudel<sup>42</sup>, L. Paul<sup>40</sup>, C.  
 231 Pérez de los Heros<sup>57</sup>, L. Peters<sup>1</sup>, J. Peterson<sup>38</sup>, S. Philippen<sup>1</sup>, D. Pieloth<sup>23</sup>, S. Pieper<sup>58</sup>, M. Pittermann<sup>32</sup>, A. Pizzuto<sup>38</sup>, M. Plum<sup>40</sup>, Y.  
 232 Popovych<sup>39</sup>, A. Porcelli<sup>29</sup>, M. Prado Rodriguez<sup>38</sup>, P. B. Price<sup>8</sup>, B. Pries<sup>24</sup>, G. T. Przybylski<sup>9</sup>, C. Raab<sup>12</sup>, A. Raisi<sup>18</sup>, M. Rameez<sup>22</sup>, K.  
 233 Rawlins<sup>3</sup>, I. C. Rea<sup>27</sup>, A. Rehman<sup>42</sup>, P. Reichherzer<sup>11</sup>, R. Reimann<sup>1</sup>, G. Renzi<sup>12</sup>, E. Resconi<sup>27</sup>, S. Reusch<sup>59</sup>, W. Rhode<sup>23</sup>, M. Richman<sup>45</sup>,  
 234 B. Riedel<sup>38</sup>, E. J. Roberts<sup>2</sup>, S. Robertson<sup>8,9</sup>, G. Roellinghoff<sup>52</sup>, M. Rongen<sup>39</sup>, C. Rott<sup>49,52</sup>, T. Ruhe<sup>23</sup>, D. Ryckbosch<sup>29</sup>, D. Rysewyk  
 235 Cantu<sup>24</sup>, I. Safa<sup>14,38</sup>, J. Saffer<sup>32</sup>, S. E. Sanchez Herrera<sup>24</sup>, A. Sandrock<sup>23</sup>, J. Sandroos<sup>39</sup>, M. Santander<sup>54</sup>, S. Sarkar<sup>44</sup>, S. Sarkar<sup>25</sup>, K.  
 236 Satalecka<sup>59</sup>, M. Scharf<sup>1</sup>, L. V. Schaufel<sup>1</sup>, H. Schieler<sup>31</sup>, S. Schindler<sup>26</sup>, P. Schlunder<sup>23</sup>, T. Schmidt<sup>19</sup>, A. Schneider<sup>38</sup>, J. Schneider<sup>26</sup>, F.  
 237 G. Schröder<sup>31,42</sup>, L. Schumacher<sup>27</sup>, G. Schwefer<sup>1</sup>, S. Sclafani<sup>45</sup>, D. Seckel<sup>42</sup>, S. Seunarine<sup>47</sup>, A. Sharma<sup>57</sup>, S. Shefali<sup>32</sup>, M. Silva<sup>38</sup>,  
 238 B. Skrzypek<sup>14</sup>, B. Smithers<sup>4</sup>, R. Snihur<sup>38</sup>, J. Soedingrekso<sup>23</sup>, D. Soldin<sup>42</sup>, C. Spannfellner<sup>27</sup>, G. M. Spiczak<sup>47</sup>, C. Spiering<sup>59,61</sup>, J.  
 239 Stachurska<sup>59</sup>, M. Stamatikos<sup>21</sup>, T. Stanev<sup>42</sup>, R. Stein<sup>59</sup>, J. Stettner<sup>1</sup>, A. Steuer<sup>39</sup>, T. Stezelberger<sup>9</sup>, T. Stürwald<sup>58</sup>, T. Stuttard<sup>22</sup>, G. W.  
 240 Sullivan<sup>19</sup>, I. Taboada<sup>6</sup>, F. Tenholt<sup>11</sup>, S. Ter-Antonyan<sup>7</sup>, S. Tilav<sup>42</sup>, F. Tischbein<sup>1</sup>, K. Tollefson<sup>24</sup>, L. Tomankova<sup>11</sup>, C. Tönnis<sup>53</sup>, S.  
 241 Toscano<sup>12</sup>, D. Tosi<sup>38</sup>, A. Trettin<sup>59</sup>, M. Tselengidou<sup>26</sup>, C. F. Tung<sup>6</sup>, A. Turcati<sup>27</sup>, R. Turcotte<sup>31</sup>, C. F. Turley<sup>56</sup>, J. P. Twagiraye<sup>24</sup>, B.  
 242 Ty<sup>38</sup>, M. A. Unland Elorrieta<sup>41</sup>, N. Valtonen-Mattila<sup>57</sup>, J. Vandenbroucke<sup>38</sup>, N. van Eijndhoven<sup>13</sup>, D. Vannerom<sup>15</sup>, J. van Santen<sup>59</sup>, S.  
 243 Verpoest<sup>29</sup>, M. Vraeghe<sup>29</sup>, C. Walck<sup>50</sup>, T. B. Watson<sup>4</sup>, C. Weaver<sup>24</sup>, P. Weigel<sup>15</sup>, A. Weindl<sup>31</sup>, M. J. Weiss<sup>56</sup>, J. Weldert<sup>39</sup>, C. Wendt<sup>38</sup>,  
 244 J. Werthebach<sup>23</sup>, M. Weyrauch<sup>32</sup>, N. Whitehorn<sup>24,35</sup>, C. H. Wiebusch<sup>1</sup>, D. R. Williams<sup>54</sup>, M. Wolf<sup>27</sup>, K. Woschnagg<sup>8</sup>, G. Wrede<sup>26</sup>, J.  
 245 Wulff<sup>11</sup>, X. W. Xu<sup>7</sup>, Y. Xu<sup>51</sup>, J. P. Yanez<sup>25</sup>, S. Yoshida<sup>16</sup>, S. Yu<sup>24</sup>, T. Yuan<sup>38</sup>, Z. Zhang<sup>51</sup>

246 <sup>1</sup> III. Physikalisches Institut, RWTH Aachen University, D-52056 Aachen, Germany247 <sup>2</sup> Department of Physics, University of Adelaide, Adelaide, 5005, Australia248 <sup>3</sup> Dept. of Physics and Astronomy, University of Alaska Anchorage, 3211 Providence Dr., Anchorage, AK 99508, USA249 <sup>4</sup> Dept. of Physics, University of Texas at Arlington, 502 Yates St., Science Hall Rm 108, Box 19059, Arlington, TX 76019, USA250 <sup>5</sup> CTSPPS, Clark-Atlanta University, Atlanta, GA 30314, USA251 <sup>6</sup> School of Physics and Center for Relativistic Astrophysics, Georgia Institute of Technology, Atlanta, GA 30332, USA252 <sup>7</sup> Dept. of Physics, Southern University, Baton Rouge, LA 70813, USA253 <sup>8</sup> Dept. of Physics, University of California, Berkeley, CA 94720, USA254 <sup>9</sup> Lawrence Berkeley National Laboratory, Berkeley, CA 94720, USA255 <sup>10</sup> Institut für Physik, Humboldt-Universität zu Berlin, D-12489 Berlin, Germany256 <sup>11</sup> Fakultät für Physik & Astronomie, Ruhr-Universität Bochum, D-44780 Bochum, Germany257 <sup>12</sup> Université Libre de Bruxelles, Science Faculty CP230, B-1050 Brussels, Belgium258 <sup>13</sup> Vrije Universiteit Brussel (VUB), Dienst ELEM, B-1050 Brussels, Belgium259 <sup>14</sup> Department of Physics and Laboratory for Particle Physics and Cosmology, Harvard University, Cambridge, MA 02138, USA260 <sup>15</sup> Dept. of Physics, Massachusetts Institute of Technology, Cambridge, MA 02139, USA

- 262 <sup>16</sup> Dept. of Physics and Institute for Global Prominent Research, Chiba University, Chiba 263-8522, Japan  
 263 <sup>17</sup> Department of Physics, Loyola University Chicago, Chicago, IL 60660, USA  
 264 <sup>18</sup> Dept. of Physics and Astronomy, University of Canterbury, Private Bag 4800, Christchurch, New Zealand  
 265 <sup>19</sup> Dept. of Physics, University of Maryland, College Park, MD 20742, USA  
 266 <sup>20</sup> Dept. of Astronomy, Ohio State University, Columbus, OH 43210, USA  
 267 <sup>21</sup> Dept. of Physics and Center for Cosmology and Astro-Particle Physics, Ohio State University, Columbus, OH 43210, USA  
 268 <sup>22</sup> Niels Bohr Institute, University of Copenhagen, DK-2100 Copenhagen, Denmark  
 269 <sup>23</sup> Dept. of Physics, TU Dortmund University, D-44221 Dortmund, Germany  
 270 <sup>24</sup> Dept. of Physics and Astronomy, Michigan State University, East Lansing, MI 48824, USA  
 271 <sup>25</sup> Dept. of Physics, University of Alberta, Edmonton, Alberta, Canada T6G 2E1  
 272 <sup>26</sup> Erlangen Centre for Astroparticle Physics, Friedrich-Alexander-Universität Erlangen-Nürnberg, D-91058 Erlangen, Germany  
 273 <sup>27</sup> Physik-department, Technische Universität München, D-85748 Garching, Germany  
 274 <sup>28</sup> Département de physique nucléaire et corpusculaire, Université de Genève, CH-1211 Genève, Switzerland  
 275 <sup>29</sup> Dept. of Physics and Astronomy, University of Gent, B-9000 Gent, Belgium  
 276 <sup>30</sup> Dept. of Physics and Astronomy, University of California, Irvine, CA 92697, USA  
 277 <sup>31</sup> Karlsruhe Institute of Technology, Institute for Astroparticle Physics, D-76021 Karlsruhe, Germany  
 278 <sup>32</sup> Karlsruhe Institute of Technology, Institute of Experimental Particle Physics, D-76021 Karlsruhe, Germany  
 279 <sup>33</sup> Dept. of Physics, Engineering Physics, and Astronomy, Queen’s University, Kingston, ON K7L 3N6, Canada  
 280 <sup>34</sup> Dept. of Physics and Astronomy, University of Kansas, Lawrence, KS 66045, USA  
 281 <sup>35</sup> Department of Physics and Astronomy, UCLA, Los Angeles, CA 90095, USA  
 282 <sup>36</sup> Department of Physics, Mercer University, Macon, GA 31207-0001, USA  
 283 <sup>37</sup> Dept. of Astronomy, University of Wisconsin–Madison, Madison, WI 53706, USA  
 284 <sup>38</sup> Dept. of Physics and Wisconsin IceCube Particle Astrophysics Center, University of Wisconsin–Madison, Madison, WI 53706, USA  
 285 <sup>39</sup> Institute of Physics, University of Mainz, Staudinger Weg 7, D-55099 Mainz, Germany  
 286 <sup>40</sup> Department of Physics, Marquette University, Milwaukee, WI, 53201, USA  
 287 <sup>41</sup> Institut für Kernphysik, Westfälische Wilhelms-Universität Münster, D-48149 Münster, Germany  
 288 <sup>42</sup> Bartol Research Institute and Dept. of Physics and Astronomy, University of Delaware, Newark, DE 19716, USA  
 289 <sup>43</sup> Dept. of Physics, Yale University, New Haven, CT 06520, USA  
 290 <sup>44</sup> Dept. of Physics, University of Oxford, Parks Road, Oxford OX1 3PU, UK  
 291 <sup>45</sup> Dept. of Physics, Drexel University, 3141 Chestnut Street, Philadelphia, PA 19104, USA  
 292 <sup>46</sup> Physics Department, South Dakota School of Mines and Technology, Rapid City, SD 57701, USA  
 293 <sup>47</sup> Dept. of Physics, University of Wisconsin, River Falls, WI 54022, USA  
 294 <sup>48</sup> Dept. of Physics and Astronomy, University of Rochester, Rochester, NY 14627, USA  
 295 <sup>49</sup> Department of Physics and Astronomy, University of Utah, Salt Lake City, UT 84112, USA  
 296 <sup>50</sup> Oskar Klein Centre and Dept. of Physics, Stockholm University, SE-10691 Stockholm, Sweden  
 297 <sup>51</sup> Dept. of Physics and Astronomy, Stony Brook University, Stony Brook, NY 11794-3800, USA  
 298 <sup>52</sup> Dept. of Physics, Sungkyunkwan University, Suwon 16419, Korea  
 299 <sup>53</sup> Institute of Basic Science, Sungkyunkwan University, Suwon 16419, Korea  
 300 <sup>54</sup> Dept. of Physics and Astronomy, University of Alabama, Tuscaloosa, AL 35487, USA  
 301 <sup>55</sup> Dept. of Astronomy and Astrophysics, Pennsylvania State University, University Park, PA 16802, USA  
 302 <sup>56</sup> Dept. of Physics, Pennsylvania State University, University Park, PA 16802, USA  
 303 <sup>57</sup> Dept. of Physics and Astronomy, Uppsala University, Box 516, S-75120 Uppsala, Sweden  
 304 <sup>58</sup> Dept. of Physics, University of Wuppertal, D-42119 Wuppertal, Germany  
 305 <sup>59</sup> DESY, D-15738 Zeuthen, Germany  
 306 <sup>60</sup> Università di Padova, I-35131 Padova, Italy  
 307 <sup>61</sup> National Research Nuclear University, Moscow Engineering Physics Institute (MEPhI), Moscow 115409, Russia  
 308 <sup>62</sup> Earthquake Research Institute, University of Tokyo, Bunkyo, Tokyo 113-0032, Japan

### 309 Acknowledgements

310 USA – U.S. National Science Foundation-Office of Polar Programs, U.S. National Science Foundation-Physics Division, U.S. National  
 311 Science Foundation-EPSCoR, Wisconsin Alumni Research Foundation, Center for High Throughput Computing (CHTC) at the  
 312 University of Wisconsin–Madison, Open Science Grid (OSG), Extreme Science and Engineering Discovery Environment (XSEDE),  
 313 Frontera computing project at the Texas Advanced Computing Center, U.S. Department of Energy-National Energy Research Scientific  
 314 Computing Center, Particle astrophysics research computing center at the University of Maryland, Institute for Cyber-Enabled Research  
 315 at Michigan State University, and Astroparticle physics computational facility at Marquette University; Belgium – Funds for Scientific  
 316 Research (FRS-FNRS and FWO), FWO Odysseus and Big Science programmes, and Belgian Federal Science Policy Office (Belspo);  
 317 Germany – Bundesministerium für Bildung und Forschung (BMBF), Deutsche Forschungsgemeinschaft (DFG), Helmholtz Alliance for  
 318 Astroparticle Physics (HAP), Initiative and Networking Fund of the Helmholtz Association, Deutsches Elektronen Synchrotron (DESY),  
 319 and High Performance Computing cluster of the RWTH Aachen; Sweden – Swedish Research Council, Swedish Polar Research Sec-  
 320 retariat, Swedish National Infrastructure for Computing (SNIC), and Knut and Alice Wallenberg Foundation; Australia – Australian

321 Research Council; Canada – Natural Sciences and Engineering Research Council of Canada, Calcul Québec, Compute Ontario, Canada  
322 Foundation for Innovation, WestGrid, and Compute Canada; Denmark – Villum Fonden and Carlsberg Foundation; New Zealand –  
323 Marsden Fund; Japan – Japan Society for Promotion of Science (JSPS) and Institute for Global Prominent Research (IGPR) of Chiba  
324 University; Korea – National Research Foundation of Korea (NRF); Switzerland – Swiss National Science Foundation (SNSF); United  
325 Kingdom – Department of Physics, University of Oxford.

POS ( ICRG2021 ) 1057